

***Cold acclimation and deacclimation in wild blueberry: direct and indirect influence of environmental factors and non-structural carbohydrates***

***Annie Deslauriers<sup>1</sup>, Léa Garcia<sup>1</sup>, Guillaume Charrier<sup>2</sup>, Valentinà Buttò<sup>1</sup>, André Pichette<sup>1</sup>, Maxime Paré<sup>1</sup>***

<sup>1</sup> Centre de recherche sur la Boréalie (CREB), Département des Sciences Fondamentales, Université du Québec à Chicoutimi, 555 boulevard de l'Université, Chicoutimi (Québec), Canada, G7H 2B1.

<sup>2</sup> Université Clermont Auvergne, INRAE, PIAF, F-63000 Clermont-Ferrand, France.

1    **Abstract**

2    Through the annual cycle of plant growth and dormancy, the winter season leads to profound metabolic  
3    changes allowing plants to undergo cold acclimation. In boreal environments, winter conditions are  
4    changing rapidly and are likely to cause damage to commercial wild lowbush blueberry. In this study, we  
5    addressed the level of frost hardiness and determined the role of environmental factors and non structural  
6    carbohydrates (NSCs) on frost hardiness. From autumn to spring, stem sections of *Vaccinium*  
7    *angustifolium* and *Vaccinium myrtilloides* were harvested each month in a commercial blueberry field to  
8    assess the relative electrolyte leakage and calculate the temperature at which 50% of the cells are lysed  
9    [ $LT_{50}$  ( $^{\circ}\text{C}$ )], used as frost hardiness index. Stems were also collected to assess soluble carbohydrates and  
10   starch. Correlations, principal component analysis (PCA) and structural equation modelling (SEM) were  
11   used to determine how environmental factors and NSCs directly or indirectly influence the frost hardiness  
12   index. Frost hardiness reached its lowest level in December and January with  $LT_{50}$  dropping below -60  
13    $^{\circ}\text{C}$ . Seasonality of frost hardening was closely linked to photoperiod and temperature, generating clock-  
14   wise hysteretic loops that divide frost hardening into acclimation, from September to January, and  
15   deacclimation, from January to the end of May. Environmental factors such as photoperiod and  
16   temperature were more important in determining the level of frost hardiness during acclimation, with  
17   either direct or indirect effect through an influence on starch degradation, increasing soluble carbohydrate  
18   content. During deacclimation, soluble carbohydrates, especially raffinose, further induced a stronger  
19   direct regulation of frost hardiness. Direct biological regulation through raffinose defined the level of frost  
20   hardiness during deacclimation. However, the negative influence of temperature on raffinose  
21   concentration could increase vulnerability to winter warming events.

22   **Keywords:** *Vaccinium angustifolium*, cold hardiness, temperature, photoperiod, snow depth, raffinose

23     **1. Introduction**

24              In boreal habitats, daily temperatures exhibit a very wide annual range: from about -40 to +30 °C.  
25     To survive harsh winter conditions, boreal shrubs inhibit their growth potential through the process of  
26     dormancy and acclimation to cold (Arora and Rowland, 2011; Charrier et al., 2011; Strimbeck et al.,  
27     2015). This process occurs in response to climate stimuli (Maurya et al., 2018; Strimbeck et al., 2008),  
28     and can thus be affected by global warming. Under climate change, winter conditions are expected to  
29     fluctuate, with higher temperature variability and increasing occurrence of polar vortices (Anderson and  
30     Gough, 2017; Yu and Zhang, 2015). Decreasing snow cover depth through a change in the balance  
31     between solid (snow) and liquid precipitations would induce more frequent freeze-thaw cycles (Williams  
32     et al., 2015). Boreal shrubs overwintering beneath the snow, such as lowbush blueberry (*Vaccinium*  
33     *angustifolium* Aiton and *Vaccinium myrtilloides* Michx), are extremely sensitive to snow cover. Indeed, a  
34     snow depth threshold of 30 cm has been identified in commercial fields in order to protect lowbush  
35     blueberry stems and buds throughout winter (Girona et al., 2019; Wildung and Sargent, 1989). In northern  
36     environments, winter damage is considered a major factor limiting blueberry fruit yields (MAPAQ, 2016;  
37     Moore, 1994). Indeed, winter warming predisposes overwintering boreal and arctic shrubs such as  
38     *Vaccinium* spp. to spring-like physiological development, possibly reducing subsequent growth,  
39     flowering, berry production or causing plant death (Bokhorst et al., 2010). Under such challenging  
40     conditions, there is a growing need to study the adaptation of plant species throughout the frost-exposed  
41     period, from autumn to spring (Arora and Taulavuori, 2016; Die et al., 2016; Palacio et al., 2015; Rowland  
42     et al., 2008). Better understanding cold acclimation and deacclimation of wild blueberry species would  
43     also help producers to better predict subsequent fruit yields when temperatures are extremely cold during  
44     autumn-spring periods.

45 In temperate and boreal environments, aboveground parts exhibit cold acclimation from autumn to winter,  
46 which transiently increases their freezing tolerance, and deacclimation from winter to spring (Charrier et  
47 al., 2013). In woody plants, cold acclimation is first initiated by decreasing photoperiod during late  
48 summer, under non-freezing temperature, and then by cold and freezing temperature in a second stage (Li  
49 et al., 2004). Compared to trees, boreal shrubs overwinter beneath the snow and thus avoid very low  
50 atmospheric temperatures. Indeed, although the environment beneath the snow is more stable, i.e.  
51 attenuation of temperature variations (Saarinen and Lundell, 2010), we have little information on the effect  
52 of temperature and snow cover on the frost hardiness of wild lowbush blueberry.

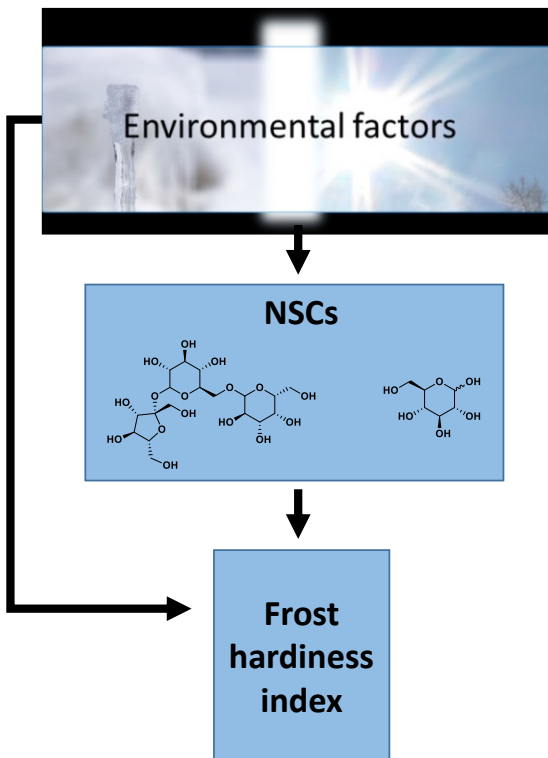
53 During cold acclimation, carbohydrates content increases as the starch reserves decrease, with opposite  
54 patterns during the period of deacclimation (Baffoin et al., 2020; Charrier et al., 2018a; Charrier et al.,  
55 2013). By increasing carbohydrate content during autumn, starch conversion indirectly contributes to  
56 freezing tolerance, as shown in *Trifolium pratense* L. (Bertrand et al., 2020). For many plant species,  
57 raffinose is an important carbohydrate for cold resistance during winter (Kasuga et al., 2007; Sauter,  
58 1988). Raffinose acts as cellular cryoprotectant allowing the stabilization of cell membranes through  
59 hydrogen bonds with membrane phospholipids, thus protecting the cell structures from frost-induced  
60 dehydration (Xin and Browse, 2000). In addition, accumulation of soluble carbohydrates in living tissues  
61 of stem and buds leads to a decrease in the freezing point, enhancing the probability of extracellular ice  
62 formation (Lee et al., 2012; Sauter, 1988). In addition to being mobile and translocated in phloem, sucrose  
63 also has a protective effect that is not based solely on osmosis effect, but also has a cryoprotective activity,  
64 stabilizing membranes and proteins (Imanishi et al., 1998), while glucose is important in providing energy  
65 for metabolism during the winter (Beauvieux et al., 2018; Die et al., 2016). The increase in solutes thus  
66 exerts a protective effect through an increase in the solute content, decreasing the freezing temperature  
67 and limiting the dehydration generated by ice formation (Baffoin et al., 2020; Charrier et al., 2013). It is

68 therefore important to understand the dynamics of the conversion between soluble carbohydrates and  
69 starch through frost acclimation and deacclimation in order to predict the frost vulnerability of *Vaccinium*  
70 spp.

71 Environmental factors such as temperature and photoperiod, can act both directly or indirectly by  
72 activating important metabolic processes (Die and Rowland, 2014; Ibáñez et al., 2010). Other  
73 environmental factors, such as snow cover, act by providing an insulating effect from extremely cold  
74 temperature (Ambroise et al., 2020; Girona et al., 2019; Palacio et al., 2015; Wildung and Sargent, 1989).  
75 In taller plants such as walnut trees, both photothermal and thermal models were able to correctly predict  
76 frost hardiness (Charrier et al., 2018a), indicating the importance of temperature and photoperiod in  
77 controlling the process involved. Even though temperature and photoperiod are correlated at higher  
78 latitudes, no additive effect (i.e. partial composition of frost hardiness under distinct temperature and  
79 photoperiod effects) was found on frost hardiness for Scots pine (Zhang et al., 2003), indicating specific  
80 and distinct roles for each of these two environmental factors.

81 In commercial wild lowbush blueberries, frost resistance studies have mainly been restricted to hybrids of  
82 *Vaccinium corymbosum* (Lee et al., 2013; Rowland et al., 2008), and the European species *Vaccinium*  
83 *myrtillus* L. (Palacio et al., 2015; Taulavuori et al., 1997). Although endemic blueberry shrubs of North  
84 America, including *Vaccinium angustifolium* Aiton and *Vaccinium myrtilloides* Michx, represent an  
85 important export for the Canadian economy [more than 200 million \$·year<sup>-1</sup> (MAPAQ, 2016)], they have  
86 rarely been investigated with respect to cold acclimation and deacclimatation (Cappiello and Dunham,  
87 1994). The study of non-structural soluble carbohydrates (NSCs), along with the key environmental  
88 parameters (photoperiod, temperature and snow depth), could therefore provide valuable information on  
89 the changes that occur in cold acclimation and deacclimation in wild blueberries. The main objectives of  
90 this study were to (1) assess the level of frost hardiness, measured as LT<sub>50</sub> (i.e. the lethal temperature at

91 which 50% of cells are lysed), in wild blueberry from autumn to spring and (2) determine the correlation  
92 between environmental factors, NSCs and frost hardiness. We tested the hypothesis that environmental  
93 factors directly influence the building NSCs for cryoprotection in the stem and that both environmental  
94 factors and NSCs are linked with the frost hardiness index (Figure 1).

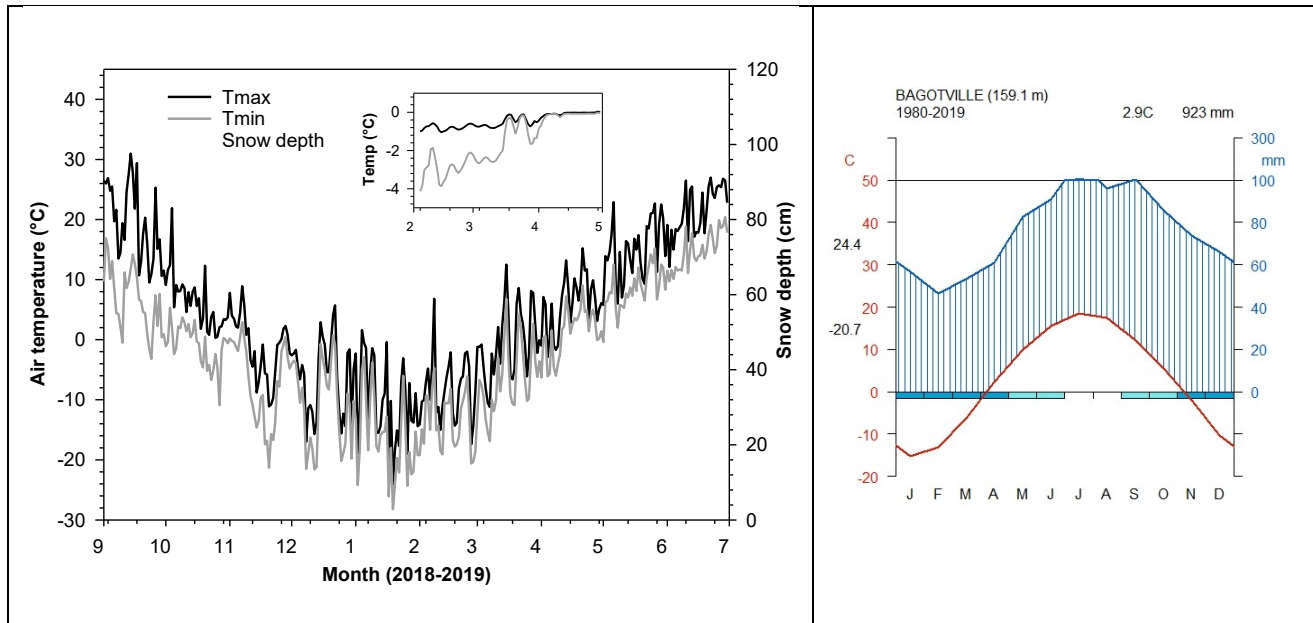


95 **Figure 1.** Assumptions behind the conceptualization of the structural equation models (SEM) linking  
96 environmental variables, NSCs and frost hardiness index. In the middle, the structure of raffinose (left)  
97 and glucose (right) represent examples of NSCs.

## 98 **2. Material and methods**

99 This study was conducted in a commercial wild lowbush blueberry field at the "Les Entreprises  
100 Gérard Doucet Ltée" in Saint-Honoré, Saguenay-Lac-Saint-Jean, Quebec, Canada (48°31'16"N;  
101 71°00'35"W, 160m a.s.l.). More than 80% of the Quebec wild blueberry fields are located in the

102 Saguenay-Lac-Saint-Jean area (MAPAQ, 2016; Vander Kloet, 1988). In this region, the climate is humid  
 103 continental with a moderately warm summer (Figure 2). Average daily temperatures range from -17 °C in  
 104 winter to 18 °C in summer (Figure 2) and minimum and maximum temperatures from -29 °C to 27 °C  
 105 (Figure 2). Because of high snow accumulation during winter [mean maximum snow cover of 77 cm from  
 106 1980 to 2019, Environment Canada (2019)], a systematic sampling design along 6 transect lines was  
 107 implemented to avoid digging beneath the snow near a previous sampling point. The use of transect lines  
 108 allow indeed to perform a systematic sampling, where samples are collected at fixed intervals of 5 meters  
 109 along each line, but at different dates (Bonham, 2013). Two transect lines per field were established in  
 110 three blueberry fields separated by mature Jack pine trees (*Pinus banksiana*, Lambs). The lines were on  
 111 each side of the field, at 13 meters from the border trees. Every month, stems of blueberry were randomly  
 112 collected (see next section) along the transect line at 5 meter intervals. During winter, a space of about 1  
 113 × 2 meters was dug in the snow to reach the plants (supplementary material, Figure S1). During sampling,  
 114 from September 2018 to June 2019, blueberry plants had both vegetative and floral buds.



115 **Figure 2.** Left part: Maximum (black line) and minimum (gray line) air temperature (°C) and snow  
 116 depth (gray background, cm) recorded at the Bagotville station from September 2018 to July 2019.

117 Inset: Mean temperature (°C) at the soil-snow interface, at two sampling points from February to May  
118 2020. Right part: Walter & Lieth climatic diagrams representing average climatic conditions [mean  
119 temperature (red line), mean precipitation (in blue)] at the nearest weather station (Bagotville). The blue  
120 rectangles represent months with below zero temperature while the cyan rectangles indicate months  
121 when below zero temperatures are highly probable.

122 Two species of wild blueberry were sampled, *Vaccinium angustifolium* Aiton and *Vaccinium myrtilloides*  
123 Michx, because species distinction was not possible beneath the snow during winter (supplementary  
124 material, Figure S1). These species also form hybrids, even having distinct genetics and phenology  
125 (Fournier et al., 2020). Both are grown together as mixed vegetation in commercial fields in the north of  
126 Quebec (Canada). At each sampling date, 24 stems were cut at the base of the plant to measure the non-  
127 structural soluble carbohydrates (NSC) concentration (4 stems × 6 transects) and 96 were cut to measure  
128 frost hardiness (16 stems × 6 transects). During sampling, performed in the morning, the plants were  
129 placed in a test tube, wrapped in wet absorbent paper around the base to prevent dehydration and kept in  
130 a cooler. In the laboratory, the stems used for NSC measurement were stored in a freezer at -17 °C for 1-  
131 2 days until liquid nitrogen immersion, while those collected for frost hardiness were treated immediately.

### 132 **2.1 Frost hardiness**

133 At each sampling date from September 2018 to June 2019, two whole stems from each transect were  
134 wrapped in moist paper and aluminum foil and exposed to controlled temperature treatments. To measure  
135 the temperature during the frost treatment, a thermocouple probe, connected to a data logger (CR100,  
136 Campbell Scientific) was placed in the middle of the blueberry stems. The stems and probes were then  
137 inserted in 7 insulated thermos and placed in a cold room (Envirotronics EH40-2-3). The temperature  
138 inside the room gradually decreased from 5 °C to -50 °C at a rate of about 5K·h<sup>-1</sup>. Seven target  
139 temperatures were selected: the first was set at 5 °C (control temperature assuming minimum damage to

140 the samples) while -1 °C, -10 °C, -20 °C, -30 °C, -40 °C and -50 °C represented progressive frost damage.  
141 Maximum damage was assumed to occur in a seventh thermos exposed to -80 °C in an ultra-low  
142 temperature freezer (Thermo Scientific, Forma 88000 Series).

143 Once the target temperature had been reached, the thermos were removed from the cold room and placed  
144 at 5 °C overnight to ensure a slow thawing. Subsequently, the buds were all removed and several small  
145 stem sections (of ~ 2-3 mm, excised between the buds) were cut with a surgical scalpel to increase  
146 electrolyte release in the solution and thereby obtain more accurate lysis values. The stem sections were  
147 then placed in a 30 ml vial filled with 10 ml of ultrapure water. A pressure of -50 bar was applied for 3  
148 minutes and then the vials were placed on stirring plates for 20 hours with gentle agitation (Lee et al.  
149 2012). Two conductivity measurements were then performed using a conductimeter (ThermoScientific  
150 Orion Star A112), before ( $C_1$ ) and after ( $C_2$ ) autoclaving the vial for 30 minutes (121 °C, 17 PSI). Relative  
151 electrolyte leakage (REL) was calculated according to the following formula:

152  $REL = \frac{C_1}{C_2}$  (1)

153 where  $C_1$  is the conductivity of the electrolyte solution measured after the cold treatment and  $C_2$  is the  
154 conductivity of the electrolyte solution measured after autoclaving.

155 The relationship between REL and temperature was then calculated according to the following four  
156 parameter sigmoidal relationships by using either each of the six transects individually or by pooling the  
157 data of all transects (Charrier et al., 2018a):

158  $REL = \frac{a}{1+e^{b(c-\theta)}} + d$  (2)

159 where  $\theta$  is the temperature ( $^{\circ}\text{C}$ ) of the cold resistance test (including controls at  $5\text{ }^{\circ}\text{C}$  and  $-80\text{ }^{\circ}\text{C}$ ), the  
160 parameters  $a$  and  $d$  define the upper (maximum lysis) and lower (minimum lysis) asymptotes of the  
161 sigmoid function and  $b$  is the nonlinear slope at the point of inflection  $c$ .

162 Between the upper and lower asymptotes, the 50% relative electrolyte leakage corresponds to the point of  
163 inflection ( $c$ ) of the sigmoid curve. This point of inflection, estimated directly by the parameter  $c$ ,  
164 corresponds to the temperature at which 50% of cells are lysed or to the lethal temperature at 50%,  $\text{LT}_{50}$   
165 ( $^{\circ}\text{C}$ ). This threshold ( $\text{LT}_{50}$ ) was used as a dynamic frost hardiness index over the winter. Parameter  
166 estimation was performed by a non-linear regression procedure (PROC NLIN) using the SAS analysis  
167 software.

168 **2.2 NSC extraction**

169 At each sampling date, the stems sampled in each transect (4 per transect) were pooled to obtain sufficient  
170 material ( $> 50\text{ mg DM}$ ) for NSC extraction (soluble carbohydrates and starch). The stems were immersed  
171 in liquid nitrogen and placed in a freeze-dryer for one week until complete desiccation. Once the samples  
172 were dry, they were ground using a ball mill (vibrating mill MM 200, Retsch).

173 For carbohydrates solubilisation, 10 mg of dry powder of stems was placed in a 15 ml test tube and mixed  
174 with 5 ml of 20% ethanol (HPLC grade) and 100  $\mu\text{l}$  of 1% sorbitol representing an internal standard. The  
175 samples were centrifuged for 10 minutes, and the supernatants were kept apart. These steps were repeated  
176 three times, but the internal standard was added only during the first extraction. The supernatant mixture  
177 was evaporated to remove the alcohol and resolubilized in 2 ml of water. The samples were then passed  
178 through an ion exchange resin: CH and N + Quaternary amino, to separate the carbohydrates and polyols  
179 from the undesired compounds. The fraction of carbohydrates and polyols was evaporated, resolubilized  
180 in 2 ml of water and then finely filtered using a nylon syringe filter (0.45  $\mu\text{m}$  pore size) and injected with  
181 HPLC-RID (Agilent 1200 series) on a Shodex SC 1011 column sugar series. The carbohydrate

182 concentrations were then determined using standard curves made for each of the identified carbohydrates:  
183 sucrose, glucose, fructose, raffinose and stachyose (Deslauriers et al., 2014).

184 The pellets recovered following carbohydrates analysis were used to measure the starch concentration  
185 (Bellasio et al., 2014). The enzymes  $\alpha$ -amylase (Megazyme - 3000 U / L), allowed the starch chains to be  
186 split into oligosaccharides and dextrans. Shorter, unbranched chains were then hydrolyzed by a second  
187 enzyme, amyloglucosidase (Megazyme - 3260 U / L). The  $\alpha$ -amylase-buffer solution (composed of 850  
188 ml of distilled water, 5.8 ml of glacial acetic acid, 1M NaOH and 0.74 g of dehydrated CaCl<sub>2</sub>) was mixed  
189 and incubated for 12 minutes at 90-100 °C. A volume of 0.15 ml of the second enzyme, amyloglucosidase,  
190 was then added and the samples were incubated for 45 minutes at 50 °C. The volume in the tubes was  
191 subsequently adjusted to 10 ml with distilled water and after being centrifuged for 6 minutes, the  
192 supernatant was recovered for subsequent analysis. Then 2 ml of Reagent solution (made from 100 ml of  
193 distilled water, 1 capsule of peroxidase (PGO) and 1.6 ml of ortho-dianisidine) was added to each of the  
194 tubes. Peroxidase (PGO) oxidized glucose to gluconic acid with quantitative production of hydrogen  
195 peroxide which in turn oxidized the dye (ortho-dianisidine). After standing for 45 minutes in the dark, 400  
196  $\mu$ L of 75% H<sub>2</sub>SO<sub>4</sub> was added, as starch is hydrolyzed in acidic condition. The absorbance was then  
197 measured after 20 min at 530 nm using a UV-VIS spectrophotometer. Starch concentrations were then  
198 converted to mg per g dry weight (mg·g<sup>-1</sup>dw).

199 **2.3 Statistical analysis**

200 In order to test our hypothesis (Figure 1), two types of analysis were conducted, principal component  
201 analysis (PCA) and structural equation modelling (SEM). While PCA aims at representing the variation  
202 between sampling dates by using all measured variables (frost hardiness index, NSCs and environmental  
203 factors), SEM aims at exploring multiple pathways by which environmental factors and NSCs determine,  
204 directly and indirectly the modulation of the frost hardiness index (Grace, 2006). For both analysis, the

205 LT<sub>50</sub> values used as a frost hardiness index, were linked to the environmental variables. Means were  
206 performed by using different time windows varying from 1 to i days prior to the sampling date with i  
207 ranging between 5 to 20 days. Mean temperature (°C), mean of daily maximum and minimum temperature  
208 (°C), mean photoperiod and mean snow depth (cm) were computed from hourly data from the Bagotville  
209 station (Environment Canada (2019). Linear correlations (Pearson, CORR procedure in SAS) were  
210 performed between LT<sub>50</sub> and the computed means to select the time window with the highest correlations.  
211 Further cross-correlations were performed by moving the different time windows from 1 to j time lag with  
212 j ranging between 1 to 55 days. The correlations between LT<sub>50</sub> and environmental factors were highest by  
213 using a window of 5 days before the sampling with no time lag (supplementary material, Figure S2).  
214 Principal component analysis (PCA) was performed to study the relationship between all the variables.  
215 Pearson's correlation coefficients between variables and axes, and contribution percentage (%) of each  
216 variable for the main PCA's axes were extracted using the R package FactoMineR (Lê et al. 2008; R Core  
217 Team 2019), while PCA was performed by means of R's package factoextra (Kassambara and Mundt  
218 2020). Direct and indirect effects of the environmental factors and NSCs on LT<sub>50</sub> were then tested by  
219 means of multi-group structural equation models (SEM), fitted separating acclimation (September to  
220 January) from deacclimation (January to May), based on the hysteresis pattern of LT<sub>50</sub> with environmental  
221 factors (see results for more detail).  
222 Models structures (Figure 1) were based according to the hypothesis that LT<sub>50</sub> depends on the interplay  
223 of both endogenous (NSCs) and exogenous factors (environment), whose influence changes according to  
224 the time of the year. Endogenous factors such as soluble carbohydrates and starch are quantitative  
225 variables that can explain frost hardiness (Bertrand et al., 2020), whereas exogenous are rather empirically  
226 correlated. The environmental factors were represented by photoperiod (hours), mean temperature (°C)  
227 and snow depth (cm). Because soluble carbohydrates were highly co-related (see result of PCA), we

228 considered that LT<sub>50</sub> was related to the amount of raffinose, because this carbohydrate is one of the most  
229 correlated with the frost hardness index (Lee et al., 2012; Sauter, 1988; Strimbeck et al., 2008). The  
230 amount of raffinose also depends on the environmental factors and amount of starch found in the plant at  
231 the same time (Lee et al., 2012). In raspberry, the increase in soluble carbohydrate was mostly explained  
232 by starch hydrolysis (Palonen et al., 2000) justifying an indirect link, via starch, between environmental  
233 factors and raffinose. In order to study the effect of each environmental factor on raffinose and on LT<sub>50</sub>,  
234 we performed three different multigroup Structural Equation Models (SEM) using one environmental  
235 variable at a time but leaving the other variables and relationships unchanged. Multicollinearity between  
236 variables was avoided by the assessment of their variance inflation factors (VIFs), retaining only those  
237 having a VIF value <10 (Zuur et al., 2010). Multigroup SEM analysis was performed by means of lavaan  
238 Rs package (Rosseel, 2012), with 10000 bootstrap resamples and Bollen-Stine bootstrapped P value (P<sub>bs</sub>)  
239 was used to test model significance as it is more adapted to small samples (Beaujean, 2014; Hooper et al.,  
240 2008). Models were accepted when P<sub>bs</sub> > 0.05. All SEM analyses were performed by means of lavaan Rs  
241 package (Rosseel, 2012), with 10000 bootstrap resamples (Beaujean, 2014). The effect of environmental  
242 factors on LT<sub>50</sub> and on NSCs concentration was assessed by comparison of the R<sup>2</sup> and the standardized  
243 coefficients (std) of their relationships in the different models.

### 244 3. Results

#### 245 3.1 Relative electrolytes leakages and LT<sub>50</sub>

246 The pattern of Relative Electrolyte Leakage (REL) changed drastically from September to October,  
247 remained similar until mid-May and then changed again (Figure 3, left panel). These fittings were  
248 performed by pooling all transect sampling points for a given date. The relations between REL and  
249 exposed temperature were all highly significant (P<0.001), except in December (P=0.036). Lower  
250 asymptotes were relatively constant ( $0.21 \pm 0.09$ ), except on December 5<sup>th</sup> and May 14<sup>th</sup>. In December,

higher minimum REL were observed compared to the other dates ( $0.45 \pm 0.04$ , Figure 3). The higher asymptotes remained relatively constant at  $0.70 \pm 0.08$ . However, from mid-May to June, the higher asymptote was much more variable, exhibiting higher (May 29) or lower values (May 14 and June 11) than 0.70. Important changes in the REL pattern mostly occurred between September and October and from April to May (Figure 3).

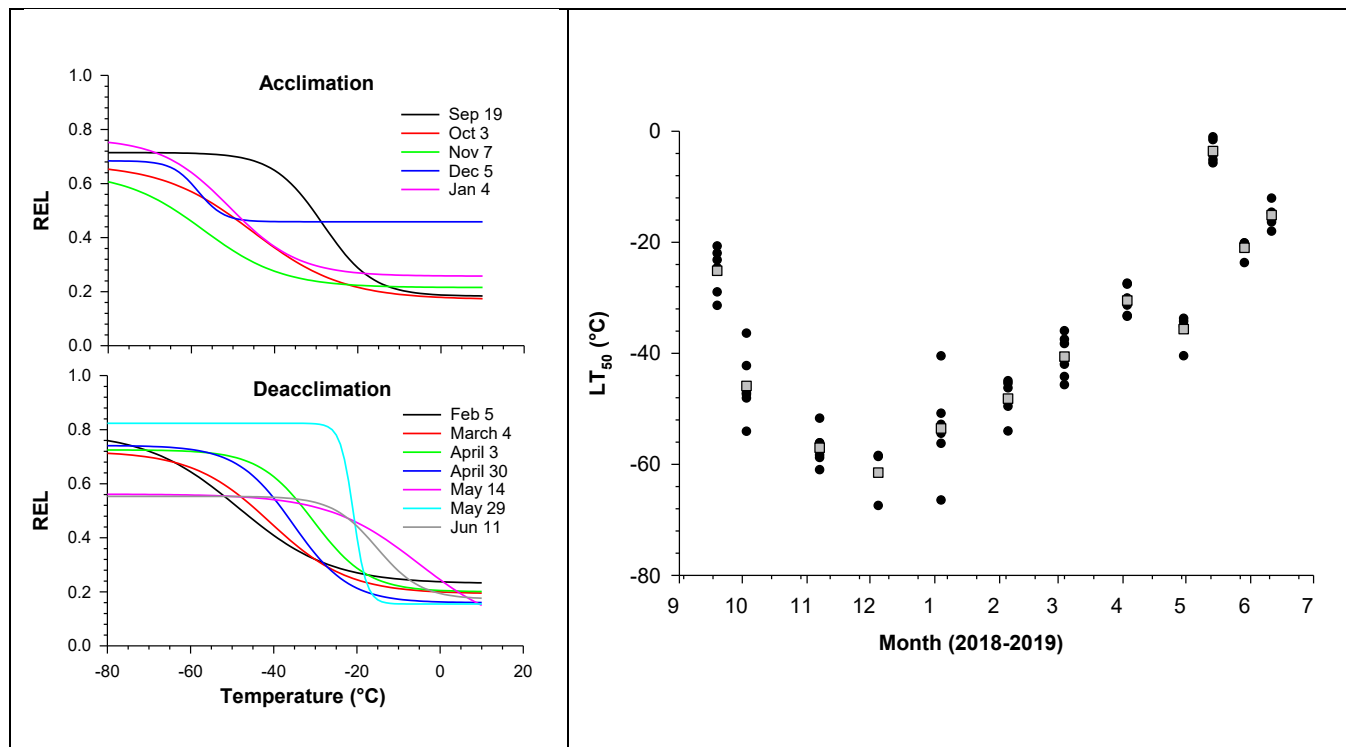


**Figure 3.** Left part: Relationships between electrolyte leakage (REL) and temperature (°C) calculated according to a sigmoidal relationship for the different sampling dates by using all transect sampling points. Curve fittings were performed by using all transect data points (black dots, illustrated in the graph on the left). Right part: LT<sub>50</sub> (°C) of each transect line (black dots) and mean LT<sub>50</sub> (gray square) for the different sampling dates.

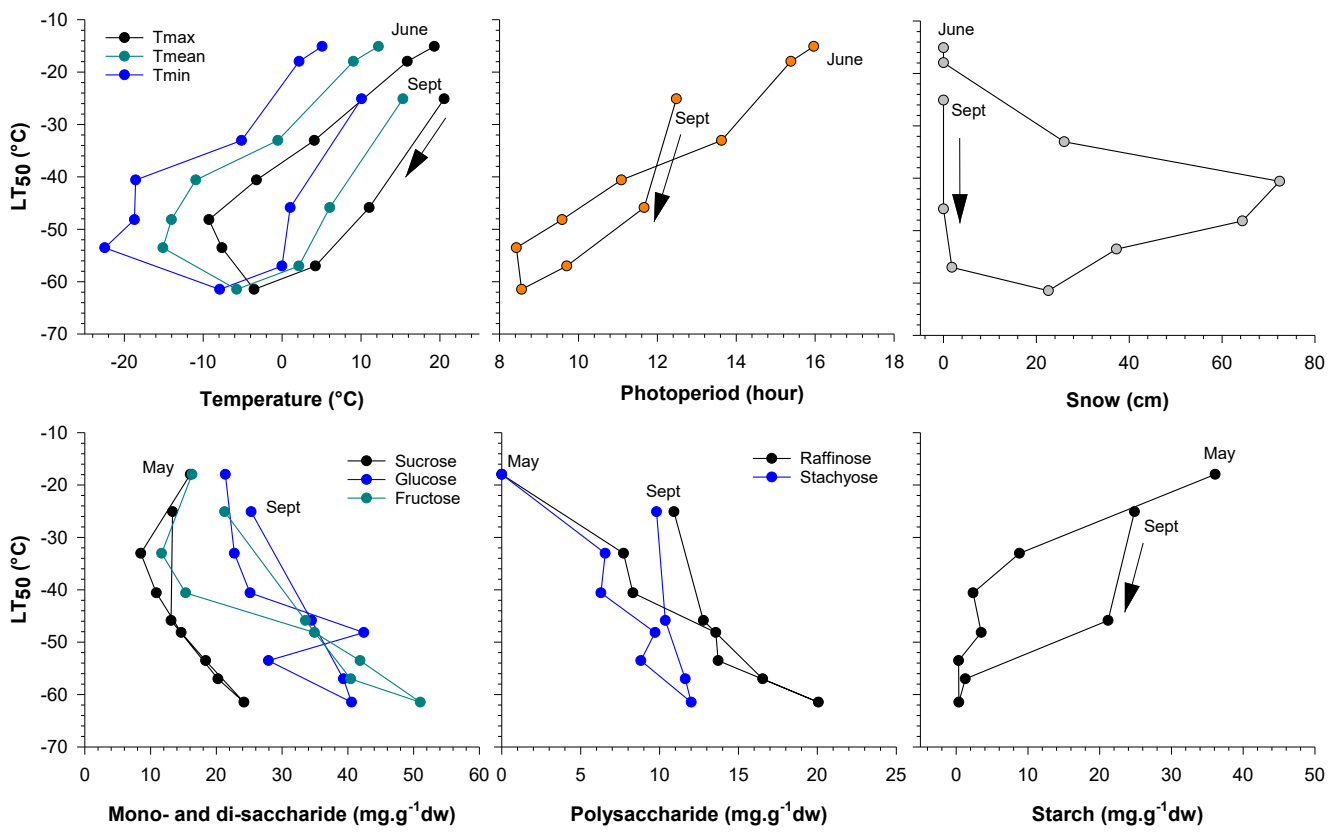
LT<sub>50</sub> in the different transects varied between -20 °C and -30 °C in September, gradually decreased in autumn to reach a minimum in December (Figure 3, right side). During the same period, the average air temperatures decreased from about 20 °C to -10 °C (Figure 2, left side). The minimum frost hardiness

264 individual values for a single plot were observed in December and January: LT<sub>50</sub> dropped to -67 °C and -  
265 66 °C in December and January, respectively (Figure 3). With only 3 fitted sigmoid regressions out of 6,  
266 the coldest frost resistance temperature was calculated on December 5<sup>th</sup>, 2018, with LT<sub>50</sub> varying between  
267 -58 °C and 67 °C. At that time, snow depth was about 20 cm and the absolute maximum and minimum  
268 air temperature recorded the week before the sampling was 0.8 °C and -14 °C, respectively (Figure 2). In  
269 January, LT<sub>50</sub> values varied between -66 °C and -40 °C, while temperatures were still decreasing but snow  
270 depth increasing (Figure 2). From January until the beginning of April 2019, LT<sub>50</sub> gradually increased.  
271 Afterwards, high LT<sub>50</sub> variability was observed. During the sampling conducted on April 30<sup>th</sup>, 2019, frost  
272 hardness dropped back to -35 °C while only traces of snow remained on the ground with air temperatures  
273 oscillating around - 5 °C (Figure 2). In mid-May, LT<sub>50</sub> reached -5 °C when minimum air temperatures  
274 approached 10 °C (Figure 2).

### 275 ***3.2 Correlation and hysteresis between LT<sub>50</sub>, NSC and environmental cues***

276 Correlation between LT<sub>50</sub> and environmental factors (mean temperature, photoperiod and snow cover),  
277 performed by using different time windows (from 5 to 20 days) and different time lags (from 0 to 55 days  
278 before the sampling) were higher by using a time window of 5 days and a time lag of 1 day (i.e. from 1 to  
279 6 days prior to the sampling) (Supplementary Figure S2). Similar results were obtained for the correlation  
280 between NSC and environmental variables, except for that between starch and photoperiod which was  
281 slightly higher at a time lag of 15 days prior to sampling. For mean temperature and photoperiod, the  
282 correlation with LT<sub>50</sub> or starch decreased with increasing time lag while the correlation increased with  
283 snow cover by increasing the time lag. For raffinose, the negative correlations increased with time lag for  
284 mean temperature and photoperiod while they decreased for snow cover. However, at lag 1, the correlation  
285 between raffinose and snow pack was very weak (Supplementary Figure S2).

286 Clockwise annual hysteresis patterns were observed between LT<sub>50</sub> and temperatures (Figure 4). For  
287 minimum, maximum and mean temperature, the decrease in LT<sub>50</sub> followed the decrease in temperature  
288 from September until December when the hysteresis loop is formed. Thereafter, LT<sub>50</sub> values increased  
289 with temperature, but with higher values compared to the previous decrease (Figure 4). The loop between  
290 photoperiod and LT<sub>50</sub> was similar to that of the temperatures but with a crossover value between  
291 September and October because of the fast decrease in photoperiod at that time of the year. On the  
292 contrary, a counter-clockwise loop was observed between snow depth and LT<sub>50</sub> (Figure 4). However, the  
293 loop with snow depth had a different form, with two direction changes between November and December  
294 (i.e. when snow started to accumulate, Figure 2) and between March and April (i.e. when snow started to  
295 melt, Figure 2). Except for starch, no hysteresis patterns were found between LT<sub>50</sub> and sugars  
296 concentrations, which rather presented a correlative pattern. For starch, hysteresis was detected with a  
297 clockwise pattern.

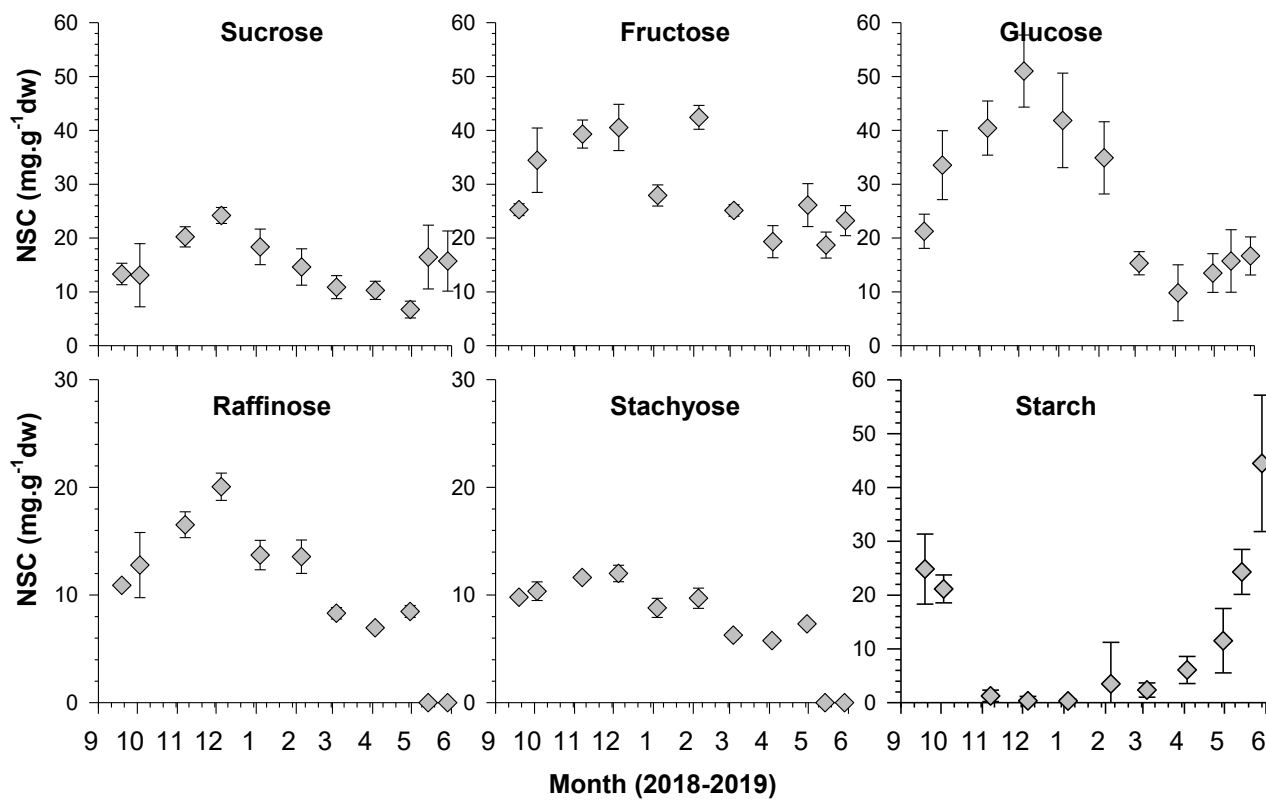


298 **Figure 4.** Higher part: Seasonal hysteresis between LT<sub>50</sub> (°C) and meteorological variables [maximum,  
 299 mean, and minimum temperature (°C) averaged over 5 days, snow depth (cm), and photoperiod (hour)]  
 300 at monthly scale. Lower part: Relationship between LT<sub>50</sub> (°C) and soluble sugars [sucrose, glucose,  
 301 fructose, stachyose and raffinose, expressed in mg.g<sup>-1</sup>dw]. Seasonal hysteresis between LT<sub>50</sub> (°C) and  
 302 starch concentration (mg.g<sup>-1</sup>dw). The direction of the hysteresis, if present, is indicated with an arrow.

303 **3.3 Carbohydrates concentration in the stem and link with LT<sub>50</sub> and environmental factors**

304 In stems, glucose, fructose sucrose and raffinose concentrations showed, more or less, a bell-shaped curve  
 305 with an increase during autumn, a maximum in December, then a decrease during winter and spring  
 306 (Figure 5). The concentrations of glucose and fructose were thus higher from November to February with  
 307 concentrations close to or higher than 40 mg.g<sup>-1</sup>dw. Both glucose and fructose had higher concentration

308 than sucrose, which reached a peak in December with about  $25 \text{ mg.g}^{-1}\text{dw}$ . The concentration of raffinose  
 309 increased from September to February with slight variations between 10 and  $20 \text{ mg.g}^{-1}\text{dw}$  then it  
 310 decreased from March and became null in May (Figure 5). Raffinose and stachyose concentrations were  
 311 low compared to the other non-structural carbohydrates. The concentration of stachyose approached 10  
 312  $\text{mg.g}^{-1}\text{dw}$ . Then, like raffinose, its concentration became null in mid-May. The starch concentration  
 313 rapidly decreased from September to October with concentration almost null from November until  
 314 January. The starch concentration then re-started to increase in February exhibiting an exponential  
 315 increase during May (Figure 5).



316 **Figure 5.** Variation in mean non-structural carbohydrates concentration (sucrose, glucose, fructose,  
 317 raffinose, stachyose and starch), expressed in  $\text{mg.g}^{-1}\text{dw}$  in blueberry shoots. Note that the scales for

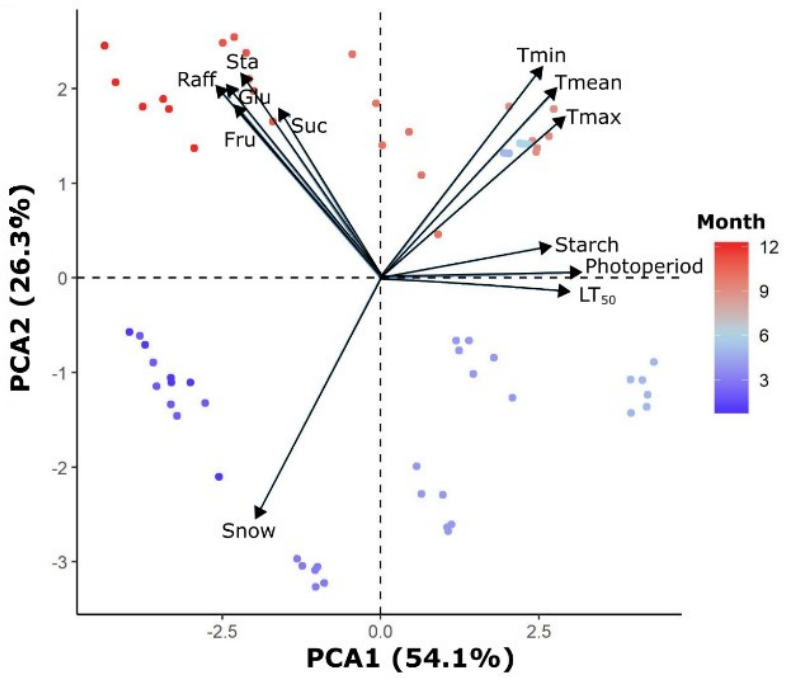
318 raffinose and stachyose differ from those for glucose, fructose, sucrose and starch. Vertical bars  
319 represent the standard deviation of the mean.

320 The PCA analysis described the relationships between variables representing the non-structural  
321 carbohydrates, LT<sub>50</sub> and environmental cues (Figure 6). The first axis (PC1), explaining 54.1% of the total  
322 variance, divides samples from low (spring and early-autumn, on the right side) to high frost resistance  
323 (winter, on the left side) according to the variables that contribute the most to PC1 (LT<sub>50</sub>, maximum  
324 temperature and photoperiod, Table 1). PC1 also defined two distinct groups of NSC: the soluble  
325 carbohydrates, negatively correlated with PC1 from starch, positively correlated with PC1 (Table 1).

326 **Table 1.** Correlation coefficients between the principal component axes PC1 and PC2 and the different  
327 variables used in the PCA with their contribution to axis definition (%).

		Variable	Correlation	P value	Contribution
PCA1	<b>Frost hardiness index</b>	LT <sub>50</sub>	0.86	<0.001	11.47
		Photoperiod	0.91	<0.001	12.87
		Tmin	0.73	<0.001	8.28
		Tmax	0.84	<0.001	10.89
		Tmean	0.80	<0.001	9.90
	<b>Environmental factors</b>	Snow	-0.57	<0.001	5.02
		Starch	0.78	<0.001	9.28
		Sucrose	-0.46	<0.001	3.25
		Glucose	-0.70	<0.001	7.51
		Fructose	-0.66	<0.001	6.77
PCA2	<b>NSCs</b>	Stachyose	-0.63	<0.001	6.15
		Raffinose	-0.75	<0.001	8.61
		<b>Frost hardiness index</b>	LT <sub>50</sub>	-0.04	0.700
			Photoperiod	0.01	0.800
			Tmin	0.64	<0.001
	<b>Environmental factors</b>	Tmax	0.49	<0.001	7.74
		Tmean	0.58	<0.001	10.59
		Snow	-0.73	<0.001	17.09
		Starch	0.1	0.400	0.30
		Sucrose	0.51	<0.001	8.30
328	<b>NSCs</b>	Glucose	0.59	<0.001	10.86
		Fructose	0.53	<0.001	8.87
		Stachyose	0.62	<0.001	12.27
		Raffinose	0.58	<0.001	10.83

329 The second axis (PC2) explaining 26% of the total variance, mostly divides the samples belonging to the  
 330 acclimation period (first part of the hysteresis loop from September until December, on the top) from the  
 331 samples belonging to the deacclimation period (second part of the loop from January until June, on the  
 332 bottom) (Figure 6). Snow, mean and minimum temperature, stachyose, raffinose and glucose were the  
 333 main variables contributing to PC2 (Table 1). The soluble carbohydrates and temperature positively  
 334 correlated with the PC2 and corresponded to the samples belonging to the acclimation period. On the  
 335 contrary, snow depth was negatively correlated with PC2 (Table 1) and corresponded to samples  
 336 belonging to the winter months (mainly from January until March) when the snow was deeper (Figure 2).



337 **Figure 6.** Principal component analysis (PCA) projecting different variables related with NSCs,  
 338 environmental cues and LT<sub>50</sub>, according to different sampling times (months, represented by dots in  
 339 different colors). Only the first two axes are represented with the relative contribution explained. Suc,  
 340 sucrose; Fru, fructose; Glu, glucose; Raff, raffinose; Sta, stachyose.

341     ***3.4 Direct and indirect influence of environmental factors and non-structural carbohydrates on LT<sub>50</sub>***

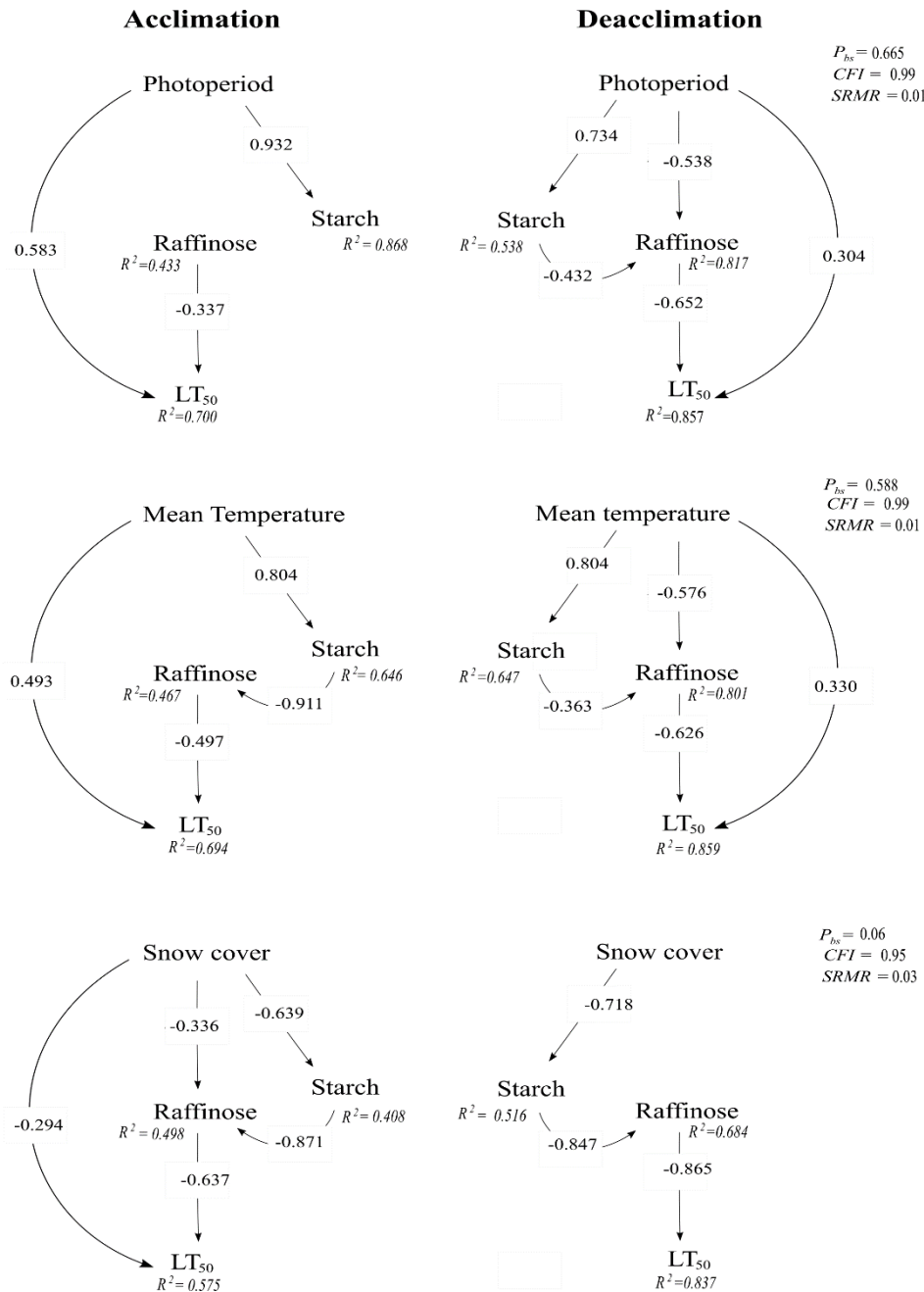
342     Based on the hysteresis pattern and PCA analysis, we divided the dataset into two groups to test the  
343     influence of environmental factors and NSCs on LT<sub>50</sub> (Figure 1): (1) cold acclimation, considering the  
344     sampling points from September 19<sup>th</sup> 2018 to January 4<sup>th</sup> 2019; (2) deacclimation, representing the period  
345     from January 4<sup>th</sup> to May 29<sup>th</sup> 2020. Because raffinose had the highest correlation with PC1, this  
346     carbohydrate was considered as representing the soluble carbohydrates dynamics in the SEM. Starch was  
347     also selected as it significantly contributed to PC1. Mean temperature was assumed to better reflect  
348     biological processes compared to minimum and maximum temperatures.

349     The SEMs suitably fitted our hypothesis ( $P_{bs}>0.05$ ,  $CFI \geq 0.95$ ,  $SRMR<0.8$ ), underlining the change in  
350     direct and indirect relationships between LT<sub>50</sub>, NSCs and environmental factors between acclimation and  
351     deacclimation periods (Figure 7, Table 2). All SEMs were similar except for the environmental variable,  
352     the relative weight of which led to changes in coefficient values of the unchanged relationships between  
353     one model and the other. Indeed, environmental factors differed in the way they affect starch and raffinose  
354     concentrations, resulting in a different setup in their direct and indirect relationships. Among the  
355     environmental factors, snow cover showed the weakest sets of goodness of fit indexes ( $p=0.06$ ,  $CFI=0.95$ ,  
356      $SMRS=0.03$ ) (Figure 7).

357     During acclimation, photoperiod, mean temperature and raffinose were highly related to LT<sub>50</sub> with  $R^2$  that  
358     varied between 0.433 and 0.868 (Figure 7). During this stage, photoperiod was the most important  
359     explanatory variable, directly and positively related to LT<sub>50</sub> ( $std=0.583$ ), meaning that LT<sub>50</sub> decreased at  
360     lower photoperiod. During acclimation, starch concentration depended on photoperiod ( $std=0.923$ ) but the  
361     variation of photoperiod and variation of starch in relation to photoperiod did not directly influence the  
362     raffinose concentration (Table 2). Mean temperature also positively influenced LT<sub>50</sub> ( $std=0.493$ ), while  
363     snow cover had the lowest effect on cold hardiness, and was negatively related to Lt<sub>50</sub> ( $std=-0.294$ ). In all

364 models,  $LT_{50}$  decreased with increasing raffinose concentration. The raffinose concentration also  
365 depended on snow cover ( $std=-0.36$ ), indicating that the concentration of this carbohydrate increased with  
366 a thinner snow cover. No direct effect of mean temperature was detected on raffinose, whose variability  
367 was explained by the variation in starch ( $std=-0.991$ ,  $R^2=0.497$ ). Starch was affected by both mean  
368 temperature and snow cover, and negatively influenced the raffinose concentration, i.e. higher  
369 concentration was measured at lower starch level. All environmental variables strongly influenced starch  
370 concentrations during acclimation: a lower starch concentration was related with a lower photoperiod  
371 ( $std=0.932$ ,  $R^2=0.868$ ) and temperature ( $std=0.804$ ,  $R^2=0.646$ ), but at deeper snow level (-0.639,  
372  $R^2=0.408$ ).

373 During the period of deacclimation (Figure 7, Table 2), the direct effects of photoperiod ( $std=0.304$ ,  
374  $R^2=0.857$ ) and temperature ( $std=0.330$ ,  $R^2=0.859$ ) were lower compared with the period of acclimation  
375 (Figure 7) and no direct effect of snow cover on  $LT_{50}$  was detected at this stage (Table 2). Compared to  
376 environmental factors, raffinose more fully explained  $LT_{50}$  during this period with coefficients ranging  
377 from -0.652 to -0.865. Raffinose was directly and negatively linked to photoperiod and mean temperature  
378 ( $std=-0.538$  and -0.576, respectively), and starch ( $std=-0.477$ ,  $R^2=0.768$ ). As during acclimation, starch  
379 was positively and directly related to photoperiod ( $std=0.734$ ,  $R^2=0.538$ ). Starch was also linked to all  
380 environmental variables in a similar way to that of acclimation with  $R^2$  varying between 0.5 to 0.9 (Figure  
381 7).



382 **Figure 7.** Structural equation model linking environmental [photoperiod, mean temperature ( $^{\circ}\text{C}$ ) and snow  
 383 cover (cm), non-structural soluble carbohydrates (raffinose and starch, in mg.  $\text{g}^{-1}\text{dw}$ ) and LT<sub>50</sub> ( $^{\circ}\text{C}$ ). Only  
 384 significant standardized coefficients are illustrated. Acclimation includes samples from September 2019  
 385 until January 2020 while deacclimation includes samples from January until May 2020. Bollen-Stine P-  
 386 values (Pbs) and goodness of fit indexes (CFI and RSMR) are provided for each model.

387 **Table 2.** Standardized coefficients (STD coefficient), STD error, z-value and P value for all SEMs  
 388 regressions.

Combination of variables	Regression	Variable	STD coefficient	STD error	z-value	P value
Photoperiod	Acclimation	LT <sub>50</sub>	Raffinose	-0.337	0.512	-2.975 <0.05
			Photoperiod	0.583	0.021	3.941 <0.001
	Deacclimation	Raffinose	Starch	-0.564	0.087	-1.701 0.089
			Photoperiod	-0.100	0.011	-0.271 0.787
	Acclimation	Starch	Photoperiod	0.932	0.09	12.714 <0.001
		LT <sub>50</sub>	Raffinose	-0.652	0.343	-5.039 <0.001
Mean temperature	Deacclimation		Photoperiod	0.304	0.011	2.786 <0.05
		Raffinose	Starch	-0.432	0.04	-3.991 <0.001
	Acclimation		Photoperiod	-0.538	0.004	-5.335 <0.001
		Starch	Photoperiod	0.734	0.011	113.558 <0.001
	Acclimation	LT <sub>50</sub>	Mean temperature	0.493	0.185	3.432 <0.01
			Raffinose	-0.497	0.468	-4.793 <0.001
Snow cover	Deacclimation	Raffinose	Starch	-0.911	0.058	-4.168 <0.001
			Mean temperature	0.317	0.066	1.368 0.171
	Acclimation	Starch	Mean temperature	0.804	0.101	8.592 <0.001
		LT <sub>50</sub>	Mean temperature	0.330	0.176	3.255 <0.001
	Deacclimation		Raffinose	-0.626	0.35	-4.847 <0.001
		Raffinose	Starch	-0.363	0.044	-3.085 <0.001
LT <sub>50</sub>	Deacclimation		Mean temperature	-0.576	0.076	-5.100 <0.001
		Starch	Mean temperature	0.804	0.187	7.187 <0.001
	Acclimation	LT <sub>50</sub>	Raffinose	-0.637	0.529	-5.435 <0.001
			Starch	-0.294	0.122	-2.132 <0.05
	Acclimation	Raffinose	Starch	-0.871	0.036	-6.306 <0.001
			Snow	-0.336	0.029	-2.298 <0.05
Raffinose	Deacclimation	Starch	Snow	-0.639	0.082	-5.824 <0.001
		LT <sub>50</sub>	Raffinose	-0.865	0.284	-8.594 <0.001
	Acclimation		Snow	-0.082	0.036	-1.137 0.255
		Raffinose	Starch	-0.847	0.063	-4.907 <0.001
	Deacclimation		Snow	-0.028	0.03	-0.158 0.874
		Starch	Snow	-0.718	0.067	-5.205 <0.001

389

390

391     **4. Discussion**

392         In wild blueberry, frost hardiness showed a transient increase and decrease from autumn to spring  
393         in response to both environmental factors and soluble carbohydrates – either directly or indirectly – in  
394         agreement with our hypothetical SEM. Our results highlighted two distinct periods of acclimation and  
395         deacclimation when environmental and biological regulation differed. Environmental factors were more  
396         closely linked to frost hardiness during cold acclimation [corresponding to the period between September  
397         and January (Charrier et al., 2011)] with a direct and indirect effect through starch degradation. This was  
398         also observed in highbush blueberry buds through protein profiling (Die et al., 2016). Autumn was  
399         characterized by the direct effect of environmental factors on starch hydrolysis increasing soluble  
400         carbohydrate contents. Later on, biological regulation, measured through soluble carbohydrates and  
401         especially raffinose, further induced a stronger direct regulation during the period of cold deacclimation,  
402         from January until the end of May at our sampling sites. Among the environmental factors, snow depth  
403         was the weakest correlated to frost hardiness, having no direct effect on raffinose concentrations during  
404         deacclimation.

405     ***4.1 Annual pattern of frost hardiness and REL curves***

406         Woody plants from boreal regions are generally highly resistant to freezing temperature and can resist a  
407         wide range of low temperature (Strimbeck et al., 2015). Short days (e.g., photoperiods) alone has been  
408         shown sufficient to induce an initial stage of frost tolerance (Arora and Taulavuori, 2016; Schwarz, 1970).  
409         Accordingly, the frost hardiness (assessed by measuring LT<sub>50</sub>) of blueberry stems already showed values  
410         <-20 °C in September. In September 2018, however, a single freeze-thaw event (minimum temperature of  
411         -0.5 °C) occurred 9 days before the first sampling date. From September 19<sup>th</sup> to October 3<sup>rd</sup>, REL curves  
412         shape changed drastically, indicating a rapid cold acclimation of the plants, early in autumn. Boreal species

413 acclimate rapidly, with the LN<sub>2</sub>-quench tolerance (i.e. surviving liquid nitrogen immersion) already  
414 acquired by late November (Strimbeck et al., 2008).

415 Maximum frost hardness was reached between November and January, between -56 °C and -67 °C.  
416 Although literature reported different acclimation timing during autumn, various highbush blueberry  
417 genotypes reach maximum cold tolerance in mid-December (Rowland et al., 2008). In December, our  
418 REL curves differed, exhibiting higher minimum REL, which could be related with native damage at the  
419 moment of sampling, even if the samples from December were treated like those from other months.  
420 Furthermore, 3 non-linear fits out of 6 samples were not significant in December while all other sampling  
421 dates had significant fitting indicating that measurements could be affected by other factors during this  
422 month. From our measurements, boreal blueberries (i.e. *V. angustifolium* and *V. myrtilloides*) can thus be  
423 considered as extreme low temperature tolerant plants [ELT, <-60 °C, Strimbeck et al. (2015)]. At our  
424 study site, the average minimum temperature in January is -22 °C with an absolute minimum that can  
425 reach -40 °C (Environment Canada, 2019). Our observations on blueberry shoots combines both bark and  
426 wood tissues, which are the most resistant organs, as observed in walnut trees (Charrier et al., 2013).

427 From April to end of May, the measured frost hardness steadily increased from -40 to almost 0 °C.  
428 *Vaccinium* spp. growing in the Alpine tundra in Switzerland exhibited similar frost hardness: between -  
429 25 °C (*Vaccinium vitis-idea* L.) and -15 °C (*V. myrtillus*) at the beginning of May (Palacio et al., 2015).  
430 However, we observed that frost hardness increased and decreased within the 15-day interval from mid-  
431 May to mid-June, with the lowest frost hardness (LT<sub>50</sub> of -3.54 °C) measured at the end of snow melt.  
432 Although only observed once in May, these variations could indicate a reacclimation pattern to cope with  
433 highly variable temperature during springtime (Arora and Rowland, 2011; Arora and Taulavuori, 2016).  
434 Rapid deacclimation in boreal areas can therefore represent an advantage to fully exploit the short  
435 favorable growing season. In our site, during the months of May-June, temperatures above 20 °C are

436 frequent, but plants can still be exposed to freezing temperatures (see probability of freezing event in May  
437 and June in the Walter & Lieth climatic diagrams, Figure 2). Sufficient and efficient reacclimation abilities  
438 are thus highly desirable traits during springtime for plant survival in a highly variable environment (Arora  
439 and Rowland, 2011).

440 **4.2 Environmental cues driving the annual pattern of frost hardiness**

441 The process of cold acclimation and deacclimation generated clock-wise hysteretic loops that were closely  
442 linked to environmental cues such as photoperiod and temperature. The influence of photoperiod  
443 represented a consistent and astronomically controlled signal that is important in anticipated response by  
444 regulating, via photoreceptors, the circadian clock (Ibáñez et al., 2010; Schultz and Kay, 2003). Exposure  
445 to short day induces the acclimation of perennial shrubs and trees to cold temperature conditions by  
446 altering the transcription of light signaling- and circadian clock-regulated genes (Maurya et al., 2018). In  
447 *Rhododendron* plants, light signal (i.e. decreasing photoperiod) before low temperature was important to  
448 further increase freezing tolerance (Liu et al., 2020), in agreement with our SEM results where photoperiod  
449 was the most correlated factor during acclimation, followed by mean temperature. Snow depth was only  
450 indirectly linked to frost hardiness through NSCs. Photoperiod was an important component of PC1 axes  
451 such as frost hardiness ( $LT_{50}$ ). As freezing is not an absolute requirement to reach low temperature  
452 tolerance in early autumn (Strimbeck et al., 2008), photoperiod is probably a predominant factor in wild  
453 blueberry in this period, followed by temperature (Li et al., 2004). Moreover, compared to temperature,  
454 the hysteretic loop related to photoperiod was narrower. Such a differential behavior could lie in the  
455 circadian clock regulation mediating the temperature-dependent processes of cold hardiness during  
456 dormancy, as observed in hybrid poplar (Ibáñez et al., 2010).

457 Both our PCA and SEM results show that air temperature represents an important factor, especially during  
458 acclimation. In trees derived from a high-elevation population of evergreen conifer *Abies sachalinensis*

459 Schmidt, frost hardiness develops earlier during acclimation compared to the low-elevation derived trees  
460 (Ishizuka et al., 2015), demonstrating stronger temperature regulation when they are colder (Liu et al.,  
461 2019). Also in walnut (*Juglans regia* L.), colder temperature accelerates the rate of frost hardening along  
462 an altitudinal gradient (Charrier et al., 2011). Earlier frost hardiness in colder sites represents an ecological  
463 adaptation by which plants reduce the length of the growing season, hence reducing the risk of frost  
464 damage (Ishizuka et al., 2015), mostly caused by the minimum temperature of freezing events (Charrier  
465 et al., 2018a). As frost events are highly probable in early September in boreal blueberry field, hardening  
466 must be reached very early in fall. Our SEM results show that the decreasing temperature during autumn  
467 also indirectly enables acclimation processes by influencing starch conversion to sugars, promoting the  
468 synthesis of cryoprotectants. At similar daily temperature, frost hardiness was much lower during  
469 acclimation than during deacclimation, generating a large hysteretic loop. In species such as *V. myrtillus*  
470 growing in northern Finland, deacclimation follows temperature and therefore already exhibits  
471 deacclimation in January (Taulavuori et al., 2002). A small rise in temperature, by 2-3 °C during winter  
472 accelerates dehardening in *V. myrtillus*, with a reduced frost hardiness in heated plants (Taulavuori et al.,  
473 1997). At our site, minimum temperatures were reached at the end of January, when LT<sub>50</sub> values has  
474 already started to increase. During deacclimation however, SEM showed that temperature has relatively  
475 minor effects, as most of the variability in frost hardiness was explained by soluble carbohydrates such as  
476 raffinose. From January to May, the regulation of frost hardiness could rely more on the internal  
477 concentration of soluble carbohydrates (see next section) or other metabolites such as increased  
478 antioxidants, proteins and amino acids (Bertrand et al., 2020; Die et al., 2016; Guy, 1990; Xin and Browse,  
479 2000), thus exhibiting inertial response (Charrier et al., 2018b).

480 The snow depth is thinner in November – December compared to the January – March period: snow  
481 started to accumulate only at mid-November and reached its peak level (about 80 cm) at the beginning of

482 March. SEM showed that snow depth was the least explanatory among the environmental factors,  
483 especially during the period of deacclimation when no direct effect of snow depth was observed on frost  
484 hardness. During acclimation however, snow depth slightly affected frost hardness (through positive  
485 correlation) and this variation was mainly driven by raffinose concentration (see next section). The deeper  
486 snow cover could offer a buffer to the variations in temperature, and especially the very low temperatures  
487 occurring in January – February, when most winter damage occurs (Girona et al., 2019). In our study, the  
488 temperature beneath the snow varied between two sampling points but was above -5 °C in February (see  
489 Figure 2, inset). However, the effect of snow depth on frost hardness was not significant in eight Ericaceae  
490 species (Palacio et al., 2015), which could explain the absence of direct effect during deacclimation. Snow  
491 removal did not cause significant short-term damage in *V. myrtillus* (Tahkokorpi et al., 2007) although the  
492 absence of snow cover in the long term caused a significant loss of this understory plants (Kreylig et al.,  
493 2012). Underground parts usually remain relatively protected by the insulating effect of snow and the  
494 thermal inertia of the soil, a decrease in snow depth can thus impair not only the aboveground parts but  
495 also roots (Ambroise et al., 2020), leading to decreased plant productivity and survival. Moreover, snow  
496 also offers protection against winter desiccation (Taulavuori et al., 2011).

497 However, measuring snow depth directly at sampling sites could have led to better correlation coefficients  
498 in SEM, as snow depth may strongly vary locally, within the same field (Girona et al., 2019). Another  
499 way to improve our models would have been to use the monitoring of air temperature underneath the snow  
500 cover, directly at the wild blueberry plant level, but our system failed to work until February. Such  
501 monitoring has the advantage of taking into consideration air temperatures and snow depth at the same  
502 time (at the same measurement), but it also has the disadvantage of reducing the applicability potential of  
503 our models, as temperature sensors are not routinely positioned beneath the snow cover for most publicly-  
504 available weather stations.

505     **4.3 Effect of non-structural carbohydrate on frost hardness**

506     Cold acclimation is often associated with changes in carbohydrates metabolism including a decrease in  
507     starch and an increase in soluble carbohydrates, such as raffinose (Beauvieux et al., 2018; Charrier et al.,  
508     2013; Kasuga et al., 2007). Starch reserves in the blueberry shoot were rapidly degraded, already reaching  
509     zero at the beginning of November. Transcripts of a protein modulating the activity of starch degrading  
510     enzymes (DSP4) in the phloem parenchyma cells remain high from autumn to spring, with highest  
511     expression during October (Berrocal-Lobo et al., 2011). In highbush blueberry (*Vaccinium corymbosum*  
512     L.), starch content also decreases in the middle of cold acclimation and coincides with  $\beta$ -amylase gene  
513     expression (Lee et al., 2012). The  $\alpha$ -amylase,  $\beta$ -amylase and starch phosphorylase activities exhibit a  
514     positive correlation with the decrease in temperature (Kasuga et al., 2007), explaining the positive  
515     influence of temperature on starch content in SEM. Shorter photoperiods during acclimation also influence  
516     starch degradation as shown by the direct effect of photoperiod on starch content in the SEM and the  
517     positive correlation of starch and photoperiod with PC1.

518     In all models (except for photoperiod during acclimation), a decrease in starch was correlated to an  
519     increase in soluble carbohydrates, such as raffinose. Raffinose was then directly and negatively correlated  
520     to frost hardness. The hydrolysis of starch stored in amyloplasts helps in producing, from starch-maltose  
521     conversion, oligosaccharides such as sucrose, raffinose and stachyose (Sauter, 1988). These soluble  
522     compounds increased in blueberry stem during autumn as the air temperature gradually dropped. Snow  
523     depth also negatively influenced raffinose content: during acclimation, beneath thinner snow, lower  
524     minimum temperatures would be reached, hence increasing raffinose content. A decoupling effect in the  
525     direct influence of photoperiod and starch raffinose concentration was observed during acclimation:  
526     raffinose was indeed strongly correlated with both photoperiod and starch ( $R_{Pearson}=-0.7$ ,  $p<0.05$ , data not

527 shown) but the direct link between starch and raffinose in the SEM model was not significant (std=-0.564,  
528 P=0.089).

529 In *V. corymbosum*, the soluble carbohydrates that were strongly associated with frost resistance were  
530 raffinose, glucose and fructose (Lee et al., 2012). In our study, stachyose was also detected with a  
531 concentration higher than 10 mg.g<sup>-1</sup>dw during winter, as also observed in boreal conifers (Strimbeck et  
532 al., 2008). Our PCA analysis revealed that stachyose was highly correlated to raffinose. In contrast,  
533 monosaccharides, especially glucose, still increased during November and December. As proposed by  
534 Beauvieux et al. (2018), the gluconeogenesis pathway can produce glucose from storage lipids and amino  
535 acids. In our study, both glucose and fructose were the most abundant solutes during the maximum of  
536 frost hardiness in December. Energy metabolism is essential to survive during a long winter as shown by  
537 an increased level of proteins involved in glycolysis during cold acclimation (Die et al., 2016). Glucose  
538 has a fundamental role during dormancy being metabolized in at least three pathways for detoxification  
539 (by the pentose phosphate pathway), mitochondrial respiration (by glycolysis) and lactate production (by  
540 fermentation) (Beauvieux et al., 2018). Therefore, glucose and fructose contents are not great predictors  
541 of frost hardiness for our *Vaccinium* species.

542 During deacclimation, our results showed that a combination of raffinose and mean temperature or  
543 raffinose and photoperiod explained a large proportion of frost hardiness variability (86 and 88%,  
544 respectively). In all models, raffinose was directly linked to frost hardiness, as observed in several boreal  
545 conifer species (Strimbeck et al., 2008). However, higher temperature directly reduced the raffinose  
546 concentration, such as during a winter warming experiment on *V. myrtillus* (Bokhorst et al., 2010),  
547 increasing the vulnerability of wild blueberries to winter warming events. Raffinose maintains membrane  
548 integrity under abiotic stress as well as ROS scavenging. Furthermore, Raffinose Family Oligosaccharides  
549 (RFOs) facilitate vitrification and prevent sucrose from crystallizing (dos Santos et al., 2011; Nishizawa-

550 Yokoi et al., 2008). Preventing sucrose crystallizing during winter desiccation, after extracellular freezing,  
551 preserves its cryoprotective effect, by maintaining the hydroxyl groups of sucrose to replace water in the  
552 phospholipid groups of the membrane (ElSayed et al., 2014; Imanishi et al., 1998). In contrast to red  
553 raspberry (Palonen et al., 2000), the disaccharide sucrose remained relatively low during winter compared  
554 to monosaccharides. However, as raffinose and stachyose are formed by the addition of a galactinol unit  
555 to sucrose (Castillo et al., 1990; Nishizawa-Yokoi et al., 2008), this could prevent sucrose concentration  
556 increasing during winter, as during drought in boreal trees (Deslauriers et al., 2014).

## 557 **5. Conclusion**

558 Multiple environmental stimuli were either directly or indirectly linked, through NSCs, to the level of  
559 frost hardening in wild blueberry *V. angustifolium* and *V. myrtilloides*. However, the importance of  
560 environmental factors differed between cold acclimation and deacclimation, being more important during  
561 acclimation when higher frost hardiness (i.e. lower LT<sub>50</sub>) is reached. Frost hardiness rapidly decreases as  
562 temperatures rise during spring making wild blueberry stems more vulnerable during deacclimation  
563 compared to the acclimation period. During the period of cold deacclimation, direct biological regulation  
564 through raffinose defined most of the frost hardiness but a negative influence of temperature on this  
565 important carbohydrate could increase vulnerability to winter warming events. In commercial wild  
566 blueberry fields, winter frost damage is a major threat and may reduce fruit yield by more than 50%, as  
567 observed in our study area in 2015 (Girona et al., 2019). As winter frost damage generally occurs during  
568 deacclimation period, our results suggest that raffinose contents could be potentially used as predictor of  
569 winter frost damage (Figure 7). Indeed, combined with air temperature data, plant raffinose content may  
570 represent a relatively easy, rapid, and quantitative way to indirectly estimate the probability of frost  
571 damage during the plant deacclimation period, and hence help producers and agronomists to better plan,  
572 at the field scale, management practices that should be performed in early spring (e.g., prescribing

573 pruning), when the buds are not yet open. Because commercial wild blueberry fields are managed over a  
574 2-year crop cycle (i.e., pruning year followed by a fruit harvesting year), not mowing damaged fields in  
575 early spring increases winter frost consequences over a longer period of time (>2 years).

576 **Acknowledgments**

577 The authors thank the Natural Sciences and Engineering Research Council of Canada (NSERC) (Grant  
578 RDCPJ-503182-16), and the *Fonds de recherche axé sur l'agriculture nordique* for their financial support.  
579 The authors also thank *Les Entreprises Gérard Doucet Ltée*, who provided access to their sites and  
580 infrastructure.

581

**References**

- Ambroise, V. et al., 2020. The roots of plant frost hardiness and tolerance. *Plant Cell Physiol.*, 61(1): 3-20.
- Anderson, C.I. and Gough, W.A., 2017. Evolution of winter temperature in Toronto, Ontario, Canada: A case study of winters 2013/14 and 2014/15. *Journal of Climate*, 30(14): 5361-5376.
- Arora, R. and Rowland, L.J., 2011. Physiological research on winter-hardiness: Deacclimation resistance, reacclimation ability, photoprotection strategies, and a cold acclimation protocol design. *Hortscience*, 46(8): 1070-1078.
- Arora, R. and Taulavuori, K., 2016. Increased risk of freeze damage in woody perennials VIS-À-VIS climate change: Importance of deacclimation and dormancy response. *Frontiers in Environmental Science*, 4: 44.
- Baffoin, R., Charrier, G., Bouchardon, A.E., Bonhomme, M. and Lacointe, A., 2020. Differential effect of carbohydrates on osmotic control of tree frost tolerance in various temperate tree species. *Tree Physiol.*, Submitted.
- Beaujean, A.A., 2014. Latent variable modeling using R: A step-by-step guide. Routledge.
- Beauvieux, R., Wenden, B. and Dirlewanger, E., 2018. Bud dormancy in perennial fruit tree species: A pivotal role for oxidative cues. *Front. Plant Sci.*, 9: 657.
- Bellasio, C., Fini, A. and Ferrini, F., 2014. Evaluation of a high throughput starch analysis optimised for wood. *PLoS One*, 9(2): e86645.
- Berrocal-Lobo, M. et al., 2011. Identification of a homolog of *Arabidopsis* DSP4 (SEX4) in chestnut: Its induction and accumulation in stem amyloplasts during winter or in response to the cold. *Plant, Cell and Environment*, 34(10): 1693-1704.
- Bertrand, A. et al., 2020. Biochemical and molecular responses during overwintering of red clover populations recurrently selected for improved freezing tolerance. *Plant Sci.*, 292: 15.
- Bokhorst, S. et al., 2010. Impacts of extreme winter warming events on plant physiology in a sub-Arctic heath community. *Physiol. Plant.*, 140(2): 128-140.
- Bonham, C.D., 2013. Measurements for Terrestrial Vegetation, Second Edition. John Wiley & Sons.
- Cappiello, P.E. and Dunham, S.W., 1994. Seasonal variation in low-temperature tolerance of *Vaccinium angustifolium* Ait. *Hortscience*, 29(4): 302-304.
- Castillo, E.M., De Lumen, B.O., Reyes, P.S. and De Lumen, H.Z., 1990. Raffinose synthase and galactinol synthase in developing seeds and leaves of legumes. *J. Agric. Food Chem.*, 38(2): 351-355.
- Charrier, G., Bonhomme, M., Lacointe, A. and Améglio, T., 2011. Are budburst dates, dormancy and cold acclimation in walnut trees (*Juglans regia* L.) under mainly genotypic or environmental control? *International journal of biometeorology*, 55(6): 763-774.
- Charrier, G., Chuine, I., Bonhomme, M. and Améglio, T., 2018a. Assessing frost damages using dynamic models in walnut trees: exposure rather than vulnerability controls frost risks. *Plant, Cell & Environment*, 41(5): 1008-1021.
- Charrier, G., Lacointe, A. and Améglio, T., 2018b. Dynamic modeling of carbon metabolism during the dormant period accurately predicts the changes in frost hardiness in walnut trees *Juglans regia* L. *Front. Plant Sci.*, 9: 1746.
- Charrier, G., Poirier, M., Bonhomme, M., Lacointe, A. and Améglio, T., 2013. Frost hardiness in walnut trees (*Juglans regia* L.): How to link physiology and modelling? *Tree Physiol.*, 33(11): 1229-1241.
- Deslauriers, A. et al., 2014. Impact of warming and drought on carbon balance related to wood formation in black spruce. *Ann. Bot.*, 114(2): 335-345.
- Die, J.V., Arora, R. and Rowland, L.J., 2016. Global patterns of protein abundance during the development of cold hardiness in blueberry. *Environ. Exp. Bot.*, 124: 11-21.
- Die, J.V. and Rowland, L.J., 2014. Elucidating cold acclimation pathway in blueberry by transcriptome profiling. *Environ. Exp. Bot.*, 106: 87-98.
- dos Santos, T.B. et al., 2011. Expression of three galactinol synthase isoforms in *Coffea arabica* L. and accumulation of raffinose and stachyose in response to abiotic stresses. *Plant Physiol. Biochem.*, 49(4): 441-448.

- 631 ElSayed, A., Rafudeen, M. and Golldack, D., 2014. Physiological aspects of raffinose family oligosaccharides in  
632 plants: protection against abiotic stress. *Plant Biol.*, 16(1): 1-8.  
633 Environment Canada, 2019. Historical climate data.  
634 Fournier, M.-P. et al., 2020. How plant allometry influences bud phenology and fruit yield in two *Vaccinium*  
635 species. *Ann. Bot.*, In press: mcaa083.  
636 Girona, J., Bradley, R., Lévesque, J.-A., Paré, M. and Bellemare, M., 2019. A call For improving winter  
637 windbreak design for lowbush blueberry production in the Saguenay–Lac-Saint-Jean region of Québec,  
638 Canada. *International Journal of Fruit Science*, 19(2): 165-178.  
639 Grace, J.B., 2006. Structural equation modeling and natural systems. Cambridge University Press, Cambridge  
640 UK.  
641 Guy, C.L., 1990. Cold acclimation and freezing stress tolerance: role of protein metabolism. *Annual Review of  
642 Plant Biology*, 41(1): 187-223.  
643 Hooper, D., Coughlan, J. and Mullen, M., 2008. Structural equation modelling: guidelines for determining model  
644 fit. *Electron J Bus Res Methods* 6: 53-60.  
645 Ibáñez, C. et al., 2010. Circadian clock components regulate entry and affect exit of seasonal dormancy as well as  
646 winter hardiness in *Populus* trees. *Plant Physiol.*, 153(4): 1823-1833.  
647 Imanishi, H.T., Suzuki, T., Masuda, K. and Harada, T., 1998. Accumulation of raffinose and stachyose in shoot  
648 apices of *Lonicera caerulea* L. during cold acclimation. *Sci. Hortic.*, 72(3-4): 255-263.  
649 Ishizuka, W., Ono, K., Hara, T. and Goto, S., 2015. Use of intraspecific variation in thermal responses for  
650 estimating an elevational cline in the timing of cold hardening in a sub-boreal conifer. *Plant Biol.*, 17(1):  
651 177-185.  
652 Kasuga, J., Arakawa, K. and Fujikawa, S., 2007. High accumulation of soluble sugars in deep supercooling  
653 Japanese white birch xylem parenchyma cells. *New Phytol.*, 174(3): 569-579.  
654 Kreyling, J., Haei, M. and Laudon, H., 2012. Absence of snow cover reduces understory plant cover and alters  
655 plant community composition in boreal forests. *Oecologia*, 168(2): 577-587.  
656 Lee, J.H., Yu, D.J., Kim, S.J., Choi, D. and Lee, H.J., 2012. Intraspecies differences in cold hardiness,  
657 carbohydrate content and  $\beta$ -amylase gene expression of *Vaccinium corymbosum* during cold acclimation  
658 and deacclimation. *Tree Physiol.*, 32(12): 1533-1540.  
659 Lee, J.I., Yu, D.J., Lee, J.H., Kim, S.J. and Lee, H.J., 2013. Comparison of mid-winter cold-hardiness and soluble  
660 sugars contents in the shoots of 21 highbush blueberry (*Vaccinium corymbosum*) cultivars. *J. Horticult.  
661 Sci. Biotechnol.*, 88(6): 727-734.  
662 Li, C., Junntila, O. and Palva, E.T., 2004. Environmental regulation and physiological basis of freezing tolerance  
663 in woody plants. *Acta Physiol. Plant.*, 26(2): 213-222.  
664 Liu, B. et al., 2020. Factors affecting freezing tolerance: a comparative transcriptomics study between field and  
665 artificial cold acclimations in overwintering evergreens. *The Plant Journal*, 103(6): 2279-2300.  
666 Liu, B., Xia, Y.-p., Krebs, S.L., Medeiros, J. and Arora, R., 2019. Seasonal responses to cold and light stresses by  
667 two elevational ecotypes of *Rhododendron catawbiense*: A comparative study of overwintering strategies.  
668 *Environ. Exp. Bot.*, 163: 86-96.  
669 MAPAQ, Ministère de l'Agriculture, des Pêcheries et de l'Alimentation du Québec., 2016. Monographie de  
670 l'industrie du bleuet sauvage au Québec. Gouvernement du Québec, pp. 32.  
671 Maurya, J.P., Triozi, P.M., Bhalerao, R.P. and Perales, M., 2018. Environmentally sensitive molecular switches  
672 drive Poplar phenology. *Front. Plant Sci.*, 9: 1873.  
673 Moore, J.N., 1994. The blueberry industry of North America. *Hort Technology* 3(4): 96-102.  
674 Nishizawa-Yokoi, A., Yabuta, Y. and Shigeoka, S., 2008. The contribution of carbohydrates including raffinose  
675 family oligosaccharides and sugar alcohols to protection of plant cells from oxidative damage. *Plant  
676 Signaling & Behavior*, 3(11): 1016-1018.  
677 Palacio, S., Lenz, A., Wipf, S., Hoch, G. and Rixen, C., 2015. Bud freezing resistance in alpine shrubs across  
678 snow depth gradients. *Environmental and Experimental Botany*, 118: 95-101.  
679 Palonen, P., Buszard, D. and Donnelly, D., 2000. Changes in carbohydrates and freezing tolerance during cold  
680 acclimation of red raspberry cultivars grown in vitro and in vivo. *Physiol. Plant.*, 110(3): 393-401.

- 681 Rosseel, Y., 2012. Lavaan: An R package for structural equation modeling and more. Version 0.5–12 (BETA).  
682 Journal of Statistical Software, 48(2): 1-36.
- 683 Rowland, L.J., Ogden, E.L., Ehlenfeldt, M.K. and Arora, R., 2008. Cold tolerance of blueberry genotypes  
684 throughout the dormant period from acclimation to deacclimation. Hortscience, 43(7): 1970-1974.
- 685 Saarinen, T. and Lundell, R., 2010. Overwintering of *Vaccinium vitis-idaea* in two sub-Arctic microhabitats: a  
686 reciprocal transplantation experiment. Polar Res., 29(1): 38-45.
- 687 Sauter, J.J., 1988. Temperature-induced changes in starch and sugars in the stem of *Populus × canadensis*  
688 «robusta». J. Plant Physiol., 132(5): 608-612.
- 689 Schultz, T.F. and Kay, S.A., 2003. Circadian clocks in daily and seasonal control of development. Science,  
690 301(5631): 326-328.
- 691 Schwarz, W., 1970. Der einfluß der photoperiode auf das austreiben, die frosthärtung und die hitzeresistenz von  
692 zirben und alpenrosen. Flora, 159(3): 258-285.
- 693 Strimbeck, G.R., Kjellsen, T.D., Schaberg, P.G. and Murakami, P.F., 2008. Dynamics of low-temperature  
694 acclimation in temperate and boreal conifer foliage in a mild winter climate. Tree Physiol., 28(9): 1365-  
695 1374.
- 696 Strimbeck, G.R., Schaberg, P.G., Fosdal, C.G., Schröder, W.P. and Kjellsen, T.D., 2015. Extreme low  
697 temperature tolerance in woody plants. Front. Plant Sci., 6: 884.
- 698 Tahkokorpi, M., Taulavuori, K., Laine, K. and Taulavuori, E., 2007. After-effects of drought-related winter stress  
699 in previous and current year stems of *Vaccinium myrtillus* L. Environ. Exp. Bot., 61(1): 85-93.
- 700 Taulavuori, K., Bauer, E. and Taulavuori, E., 2011. Overwintering stress of *Vaccinium vitis-idaea* in the absence  
701 of snow cover. Environ. Exp. Bot., 72(3): 397-403.
- 702 Taulavuori, K., Laine, K. and Taulavuori, E., 2002. Artificial deacclimation response of *Vaccinium myrtillus* in  
703 mid-winter, Annales Botanici Fennici. JSTOR, pp. 143-147.
- 704 Taulavuori, K., Laine, K., Taulavuori, E., Pakonen, T. and Saari, E., 1997. Accelerated dehardening in bilberry  
705 (*Vaccinium myrtillus* L.) induced by a small elevation in air temperature. Environ. Pollut., 98(1): 91-95.
- 706 Vander Kloet, S.P., 1988. The genus *Vaccinium* in North America. Agriculture Canada, Gouvernement du  
707 Canada, 218 pp.
- 708 Wildung, D.K. and Sargent, K., 1989. The effect of snow depth on winter survival and productivity of Minnesota  
709 blueberries. Acta Horticulturae(241): 232-237.
- 710 Williams, C.M., Henry, H.A. and Sinclair, B.J., 2015. Cold truths: how winter drives responses of terrestrial  
711 organisms to climate change. Biological Reviews, 90(1): 214-235.
- 712 Xin, Z. and Browne, J., 2000. Cold comfort farm: the acclimation of plants to freezing temperatures. Plant, Cell &  
713 Environment, 23(9): 893-902.
- 714 Yu, B. and Zhang, X., 2015. A physical analysis of the severe 2013/2014 cold winter in North America. Journal  
715 of Geophysical Research: Atmospheres, 120(19): 10,149-10,165.
- 716 Zhang, G., Ryypö, A., Vapaavuori, E. and Repo, T., 2003. Quantification of additive response and stationarity of  
717 frost hardiness by photoperiod and temperature in Scots pine. Can. J. For. Res.-Rev. Can. Rech. For.,  
718 33(9): 1772-1784.
- 719 Zuur, A.F., Ieno, E.N. and Elphick, C.S., 2010. A protocol for data exploration to avoid common statistical  
720 problems. Methods in Ecology and Evolution, 1: 3-14.

721

722 **Captions ‘list**

723 **Figure 1.** Assumptions behind the conceptualization of the structural equation models (SEM) linking  
724 environmental variables, NSCs and frost hardiness index. In the middle, the structure of raffinose (left)  
725 and glucose (right) represent examples of NSCs.

726 **Figure 2.** Left part: Maximum (black line) and minimum (gray line) air temperature ( $^{\circ}\text{C}$ ) and snow  
727 depth (gray background, cm) recorded at the Bagotville station from September 2018 to July 2019.  
728 Inset: Mean temperature ( $^{\circ}\text{C}$ ) at the soil-snow interface, at two sampling points from February to May  
729 2020. Right part: Walter & Lieth climatic diagrams representing average climatic conditions [mean  
730 temperature (red line), mean precipitation (in blue)] at the nearest weather station (Bagotville). The blue  
731 rectangles represent months with below zero temperature while the cyan rectangles indicate months  
732 when below zero temperatures are highly probable.

733 **Figure 3.** Left part: Relationships between electrolyte leakage (REL) and temperature ( $^{\circ}\text{C}$ ) calculated  
734 according to a sigmoidal relationship for the different sampling dates by using all transect sampling  
735 points. Curve fittings were performed by using all transect data points (black dots, illustrated in the  
736 graph on the left). Right part:  $\text{LT}_{50}$  ( $^{\circ}\text{C}$ ) of each transect line (black dots) and mean  $\text{LT}_{50}$  (gray square)  
737 for the different sampling dates.

738 **Figure 4.** Higher part: Seasonal hysteresis between  $\text{LT}_{50}$  ( $^{\circ}\text{C}$ ) and meteorological variables [maximum,  
739 mean, and minimum temperature ( $^{\circ}\text{C}$ ) averaged over 5 days, snow depth (cm), and photoperiod (hour)]  
740 at monthly scale. Lower part: Relationship between  $\text{LT}_{50}$  ( $^{\circ}\text{C}$ ) and soluble sugars [sucrose, glucose,  
741 fructose, stachyose and raffinose, expressed in  $\text{mg.g}^{-1}\text{dw}$ ]. Seasonal hysteresis between  $\text{LT}_{50}$  ( $^{\circ}\text{C}$ ) and  
742 starch concentration ( $\text{mg.g}^{-1}\text{dw}$ ). The direction of the hysteresis, if present, is indicated with an arrow.

743 **Figure 5.** Variation in mean non-structural carbohydrates concentration (sucrose, glucose, fructose,  
744 raffinose, stachyose and starch), expressed in  $\text{mg.g}^{-1}\text{dw}$  in blueberry shoots. Note that the scales for

745 raffinose and stachyose differ from those for glucose, fructose, sucrose and starch. Vertical bars  
746 represent the standard deviation of the mean.

747 **Figure 6.** Principal component analysis (PCA) projecting different variables related with NSCs,  
748 environmental cues and LT<sub>50</sub>, according to different sampling times (months, represented by dots in  
749 different colors). Only the first two axes are represented with the relative contribution explained. Suc,  
750 sucrose; Fru, fructose; Glu, glucose; Raff, raffinose; Sta, stachyose.

751 **Figure 7.** Structural equation model linking environmental [photoperiod, mean temperature (°C) and  
752 snow cover (cm), non-structural soluble carbohydrates (raffinose and starch, in mg. g<sup>-1</sup>dw) and LT<sub>50</sub>  
753 (°C). Only significant standardized coefficients are illustrated. Acclimation includes samples from  
754 September 2019 until January 2020 while deacclimation includes samples from January until May 2020.  
755 Bollen-Stine P-values (Pbs) and goodness of fit indexes (CFI and RSMR) are provided for each model.

756 **Table 1.** Correlation coefficients between the principal component axes PC1 and PC2 and the different  
757 variables used in the PCA with their contribution to axis definition (%).

758 **Table 2.** Standardized coefficients (STD coefficient), STD error, z-value and P value for all SEMs  
759 regressions.

760

761

## Supplementary Figures

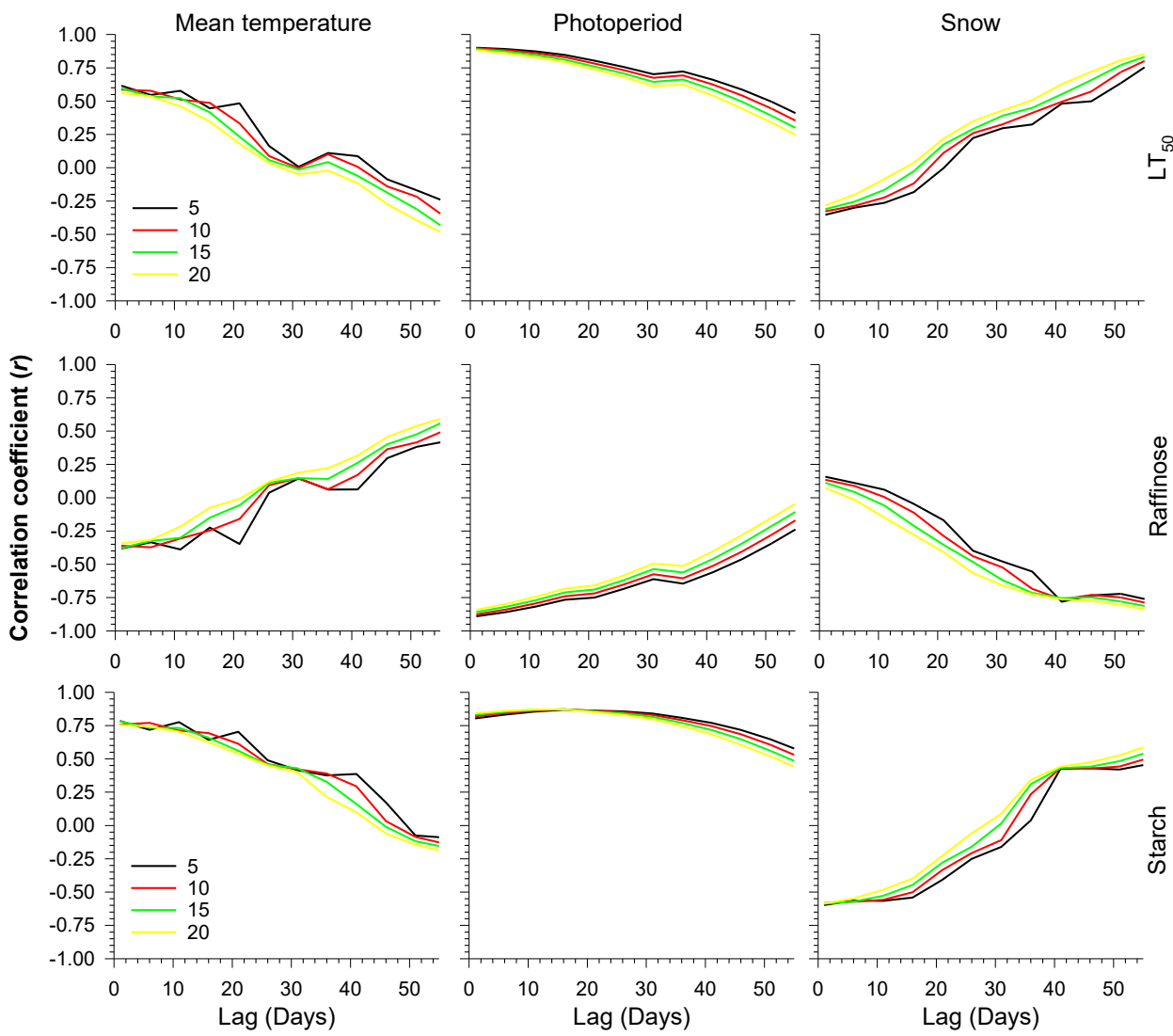
762



763 **Figure S1.** Sampling at one transect point in February. The blueberry stems were dig up by removing  
764 the snow in a surface of about 2 meters long × 1 meter large. The higher portion of one stem was cut due  
765 to ice formation at the soil surface. It was not possible to distinguish the stems belonging to the species  
766 *Vaccinium angustifolium* or *Vaccinium myrtilloides* under the snow during winter. Therefore, both  
767 species were simultaneously sampled.

768

769



770

771 **Figure S2.** Variation of the correlation coefficient ( $r$ , Pearson) between  $LT_{50}$ , raffinose and starch and  
 772 environmental variables (mean temperature, photoperiod and snow level). We use different time  
 773 windows (between 5 and 20 days) to calculate means environmental parameters and different time lag  
 774 (from 1 to 55 days) before the sampling. For example, for a window of 5 day, we calculate mean  
 775 environmental parameter by including the 1<sup>st</sup> to the 6<sup>th</sup> day prior to the sampling at lag 1, then the  
 776 second to the 7 at lag 2. Then, the different combination of time window and lag were correlated either  
 777 with  $LT_{50}$  or NSC values.

778